Laser development of rare-earth doped crystals

N.D. Vieira Jr.[a],[*], I.M. Ranieri[a], L.V.G. Tarelho[a], N.U. Wetter[a], S.L. Baldochi[a], L. Gomes[a],
P.S.F. de Matos[a], W. de Rossi[a], G.E.C. Nogueira[a], L.C. Courrol[b], E.A. Barbosa[b], E.P. Maldonado[c],
S.P. Morato[c]

[a]*Centro de Lasers e Aplicações, IPEN, Travessa R, 400-Cidade Universitária, CEP 05508-900, São Paulo, Brazil*
[b]*FATEC, Pça Coronel Fernando Prestes, 30-CEP 01124-060, São Paulo, Brazil*
[c]*LASERTOOLS, CP 11049, Butantã, 05422-970, São Paulo, Brazil*

Abstract

Rare earth doped laser crystals present good optical properties providing most of the solid state lasers available today. In particular, some fluoride crystals are capable of forming solid solution with several rare earth fluorides, allowing one to take full advantage of the energy transfer mechanisms that might occur among them. $LiREF_4$ (RE=rare earth) crystals, for example, are so flexible that in some cases the doping concentration can go up to 100%. The $Nd:LiLuF_4$ (Nd:LuLF) system has a 1047-nm emission bandwidth 25% larger than Nd:YLF, which makes it very promising for laser mode-locked operation. Nevertheless, lutetium compounds are very difficult to obtain, therefore Nd-doped mixed crystals grown from $LiF-Y_{1-x}Lu_xF_3$ ($0 < x < 1$) solid solutions were studied. A new laser medium was obtained for the $Nd:LiLu_{0.5}Y_{0.5}F_4$ crystal, which presents a Nd emission bandwidth close to the Nd:LuLF (1.82 nm). The mode-locked operation in a diode pumped laser system using the KLM technique was performed and pulses of 4.5 ps were readily obtained. It is also shown that the $LiGdF_4$ (GLF) is a promising host for diode pumped high power Nd lasers which require crystals with higher dopant concentrations. Another example is the $Ho:LiYF_4$ (Ho:YLF) laser operating at 2065 nm obtained as a result of concentration optimization of the sensitizers Er and Tm. The optimization was based on a model comprising the various energy transfer mechanisms that take place in these long lived metastable states, heavily dependent on the dopants concentration. As a quasi-four-level system, the Ho concentration must be kept very small (≤ 0.005 mol%). The laser operation was optimized by the dynamical coupling of pump and laser modes, and by the dopants optical cycle. These optimizations resulted in a CW Ho laser with 2 W output, in a diode pumped system operation.
© 2002 Elsevier Science B.V. All rights reserved.

Keywords: Rare earth alloys and compounds; Crystal growth; Luminescence; Time-resolved optical spectroscopies; Light absorption and reflection

1. Introduction

Solid-state lasers emitting at 1 and 2 µm have various applications in a wide range of fields, including LIDAR, dental caries prevention and air turbulence detection. Laser radiation applied to the surface of human dental enamel has shown to increase resistance against caries, reduce sensitivity to pain and improve microhardness and also roughness for better bond strength of composite resin restorations [1,2]. Doppler LIDAR systems operating at 2 µm are currently used to detect aerosol flow. Typical detection ranges are up to 3 km, with a laser specification of 2 mJ pulse energy, 200-ns pulse duration and at least 10 Hz repetition rate. Using low loss, externally triggered acousto-optic modulators, these specifications can be obtained once the laser generates more than 1.5 W of peak power in the quasi CW regime [3,4].

Nd ion based lasers are among the mostly used solid-state laser systems. They find applications in many areas, including the generation of the highest energy per pulse for laser fusion purposes. However, one of the main limitations in the crystalline hosts is the available bandwidth of the laser transition that limits the minimum pulse duration to ~1 ps. In this work, we have explored the potential of growing new Nd hosts, performed the spectroscopic characterization of them and investigated their laser properties. A new mixed crystal, Nd:LuYLF, was grown with high optical quality. CW and mode-locked regime laser operation were demonstrated to explore this broader emission band.

The Tm:Ho:YLF laser emitting at 2.06 µm is a quasi-three-level system with a non-negligible thermal popula-

*Corresponding author. CP 11049, Butantã, CEP 05422-970, São Paulo, Brazil. Tel.: +55-11-3816-9301; fax: +55-11-3816-9315.

E-mail address: nilsondv@net.ipen.br (N.D. Vieira Jr.).

tion of the lower laser level resulting in considerable reabsorption at room temperature [5]. One way to circumvent this is to use cooperative effects by growing crystals with low Ho concentration codoped with another RE ion. In the system the Ho ions act as the acceptor and the RE ions as the donors, being also responsible for the absorption of pumping light. Additionally, the system has up-conversion processes in both thulium and holmium, which reduce the population of the upper laser level [6]. The net effect of up-conversion losses is an increase in the threshold pump power, whereas reabsorption losses result in lower slope efficiencies. Both effects can be significantly decreased by cooling the crystal below -27 °C and employing a pump distribution, which spreads the absorption uniformly over the whole crystal length by pumping it from both sides [3].

Another technique that offsets these adverse effects is to use a quasi-CW pumping of the crystal, allowing operation at crystal temperatures above 0 °C. The main advantage of this technique is a simpler architecture of the laser resonator since there is no need for a nitrogen-purged enclosure of the crystal or a double side pumping technique. Furthermore, cooling off the diode bar and the crystal can be done by thermoelectric elements. Besides, it has been shown [6] that Tm:Ho:YLF has relatively small up-conversion losses under Q-switched operation when compared to Tm:Ho:YAG [6]. Therefore, pumping the crystal with higher intensities should permit a higher gain, which in turn permits higher pulse energies and a shorter pulse duration [7].

2. Experimental

2.1. Crystal preparation

Laser crystals must have high optical quality, this involves the use of high-purity raw materials and adequate crystal growth conditions. In general, the raw materials were obtained from pure rare earth oxide powders (99.9% or better) by hydrofluorination at high temperature in HF atmosphere. The powder is placed in a cylindrical platinum boat, enclosed by a sealed platinum tube. The LiF-REF$_3$ mixtures are melted using an open platinum boat in the HF atmosphere, with the peritectic composition, according to the phase diagram of each system. LiF powder (99.9% or better) is also zone-refined before it is added to the REF$_3$. Pure commercial powders (99.99% or better) can be utilized if a reactive atmosphere, such as CF$_4$, is used during crystal growth process [8–10]. Besides the reaction of rare earth fluorides with oxygen and moisture, the raw materials must be free of organic matter that can remain from the rare earth synthesis. Otherwise, the melt surface present a carbon scum, making the seeding process sometimes impossible [8]. Single crystals have been grown by the Czochralski technique under high purity argon

(99.9995%). The crystal-pulling rates were 0.5–1 mm/h, with 8–30 rpm rotation rates. Two kinds of solid solutions have been investigated, one kind was for the development of Nd lasers and the other one for Ho lasers.

LiGd$_{1-x}$Nd$_x$F$_4$ crystals and LiY$_{1-x}$Nd$_x$F$_4$ with concentrations in the melt of $x=0.027$ were grown for spectroscopic studies. New solid solutions of LiY$_{1-x-y}$Lu$_x$Nd$_y$F$_4$ were obtained with $x=0.09$, 0.31, 0.473 and 1 and $y=0.023$ or 0.027 for spectroscopic studies and laser testing. Small crystals of good optical quality weighing around 50 g were obtained, except for the LuLF where only a 10-g crystal was obtained.

LiY$_{1-x-y-z}$Er$_x$Tm$_y$Ho$_z$F$_4$ crystals with $0<x<0.4$, $0.01<y<0.20$ and $0.001<z<0.1$ were grown for the spectroscopic studies of energy transfer to optimize the laser output for flash-lamp and diode laser pumping [11].

2.2. Optical characterization

The absorption cross-sections were determined by the unpolarized optical absorption spectrum. This orientation avoids polarization effects to the experimental data. The absorbance spectra of Nd, Er, Tm and Ho samples were measured in a double beam spectrophotometer automated CARY 17 D from OLIS.

The crystal was pumped by a GaAlAs laser diode (SDL-2382-P1) which is a broad-area CW laser (1×500 μm), with 4 W power, operating at 797 nm. The diode laser beam was collimated by a diffraction-limited, NA= 0.5, $f=8$ mm objective, corrected by a ×3 anamorphic prism pair (both from Melles Griot) and focused by a single $f=10$-cm lens. Close to the focus, and for a longitudinal range of 2 mm, the beam had a rectangular profile, with transverse dimensions of approximately 60× 300 μm. The pumping excitation was in the π orientation.

For the emission measurements, the crystal was pumped either by the diode laser or by the Xenon lamp. Both light beams, chopped at 40 Hz, were focused on the sample with a 10-cm focal length lens. The visible Nd emission was detected with an EMI 9558 photomultiplier and analyzed with a 0.25-m (Kratos) monochromator. The luminescence signal was processed using a PAR lock-in amplifier. The lifetimes of excited Nd^{3+} ions were measured using a pulsed laser excitation (10 ns) from a nitrogen laser pumped dye laser tuned at 413 nm. The time-dependent signal was detected by a fast S-20 extended-type photomultiplier and analyzed using a signal-processing Box–Car averager (PAR 4402).

All spectroscopic and laser samples were extracted along the growth direction. The optimum active medium length for longitudinally pumped at 792 nm Nd:YLF lasers is approximately 1 cm, for Nd concentrations around 1 mol%, and considering high quality pumping sources [12]. For high-power diode laser pumping, however, the high M^2 factor of the laser beam limits the effective pumping length. Despite this pumping problem, and considering a

four-level laser model for the 1047-nm Nd laser transition, we prepared active elements 1-cm long, with transversal dimensions of approximately (0.2×0.5) cm. The optical facets were prepared at Brewster angle for the π polarization, and polished to a flatness of $\lambda/4$. The transmission of the laser samples around 1050 nm was better than 0.995(5) for both Nd:YLF and Nd:LuYLF laser crystals.

The excitation system for the Er, Tm and Ho samples consists of a second harmonic generator pumped by a Quantel Nd:YAG pulsed laser (800 mJ, 4 ns, 10 Hz) that pumps an OPOTEK optical parametric oscillator. The tunability of the OPO allowed excitation wavelengths at the range of 680–1000 and 1200–2000 nm.

The visible and near infrared emissions for the Er, Tm and Ho samples were properly injected and dispersed by a 0.25-m SPEX monochromator. The visible light was detected by a S-20 EMI photomultiplier coupled to a Tektronix digital oscilloscope connected to a computer via GPIB interface. The infrared emissions were focused into a Judson InSb detector whose signal was amplified and connected to the oscilloscope. This experimental setup allowed investigations of temporal dynamics and time resolved emission spectra of the crystalline samples in order to develop the optimization process.

3. Results

3.1. Spectroscopic studies

3.1.1. Nd systems

Lutetium is a well-known size-compensating codopant for Nd:YAG (Nd:$Y_3Al_5O_{12}$) laser crystals, allowing the incorporation of greater amounts of Nd into YAG without significant degradation of the optical quality, and broadening the emission lines by around 10–35% [13]. Recently, a new fluoride laser material has been grown: Nd:LuLF [14]. This material presents almost the same spectral and physical properties as Nd:YLF laser crystals, but presents broader spectral width. Broadening the spectral gain width is a desirable enhancement for crystalline Nd laser media in order to obtain short pulses, especially when using passive mode-locking techniques. In this case, the minimum pulse width, obtained by balancing the nonlinear phase effects with net group-velocity dispersion, is inversely proportional to the square of the gain spectral linewidth [15,16].

We have studied the codoping of lutetium in Nd:YLF crystals in order to obtain significant line broadening and enhanced Nd concentration, also aiming to lower the production costs compared with those of Nd:LuLF. We verified that, by using 50% of lutetium and 50% of yttrium, the obtained laser crystal presented the same physical and spectroscopic parameters, and a significant spectral broadening of the emission linewidth, compared with Nd:YLF (at 1047 nm). We named this laser material

Nd:LuYLF. The measured $^4F_{3/2}$ lifetimes were 481 and 476 ms for Nd:LuYLF and Nd:YLF, respectively.

The emission and absorption spectra of both Nd:LuYLF and Nd:LuLF are similar to those of Nd:YLF. Excitation in both cases were done by 792 nm diode laser line. The emission cross-sections for the $^4F_{3/2} \rightarrow ^4I_{11/2}$ transitions (π and σ polarizations), were obtained by using the method of McCumber [17]. The peak emission cross-sections for Nd:LuYLF were determined and the values are 1.96×10^{-19} cm^2 at 1046 nm (π polarization), and 1.49×10^{-19} cm^2 at 1052 nm (σ polarization). A detailed measurement of the fluorescent emission spectrum around 1047 nm for Nd:YLF, Nd:LuYLF and Nd:LuLF allowed the determination of the spectral linewidths presented in Fig. 1. The plotted line is an empirical fit for different Lu concentrations. We readily notice that Nd:LuYLF has almost the same emission linewidth as Nd:LuLF, broadened approximately by 25% compared with that of the Nd:YLF sample, under this high intensity diode laser pumping.

The spectroscopic properties of Nd in GLF are very similar to those of Nd:YLF, however GLF host allows higher concentrations of Nd^{3+} than in YLF. Nd:GLF laser also present low threshold and high efficient laser action under pulsed and CW pumping [18,19].

Analysis of the oscillator strengths for dipole-forced electronic transitions of 3+ rare-earth ions in solids is widely used by applying the Judd–Ofelt theory [20]. We used the same approach to calculate Ω_t in Nd:GLF as has been done for Nd:YLF crystal [21]. The calculated values of Ω_t for Nd:GLF are:

$$\Omega_2 = 0.905 \times 10^{-20} \text{ cm}^2$$

$$\Omega_4 = 2.47 \times 10^{-20} \text{ cm}^2$$

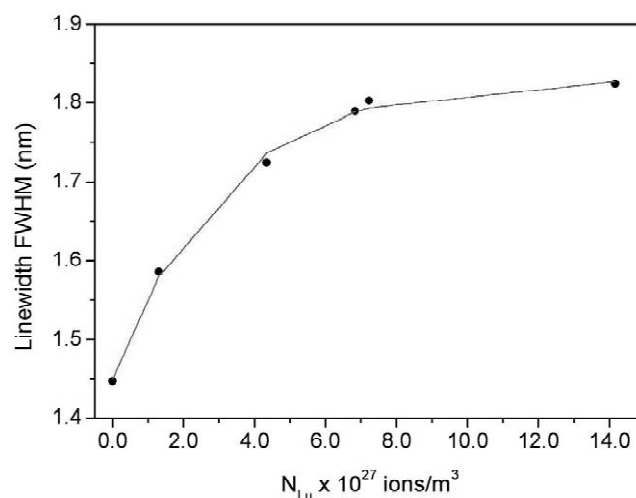$$\Omega_6 = 4.92 \times 10^{-20} \text{ cm}^2$$

Fig. 1. Measured spectral linewidths at the 1047-nm emission (π), for Nd:Lu:YLF crystals with different Lu concentrations.

By using the Ω_t values and the matrix elements $U^{(t)}$ for Nd^{3+} obtained from the literature (W.T. Carnall, H. Crosswhite, H.M. Crosswhite, unpublished data), it was possible to calculate the radiative transition probabilities for all the up-conversion processes and emissions relevant for the diode pumped Nd-laser system. One can compute the total radiative rate of the transitions ending below the metastable $^4F_{3/2}$ level $(\tau_{31})^{-1}$, and the total rates of radiative transitions contributing for the $^4F_{3/2}$ population $(\tau_{32})^{-1}$. The radiative transitions contributing for $(\tau_{31})^{-1}$ are those from $^4G_{7/2}$ to $^4I_{9/2}$, $^4I_{11/2}$, $^4I_{13/2}$ and $^4I_{15/2}$, respectively. The radiative transitions from $^4G_{7/2}$ to $^2H_{9/2}$ and $^4F_{3/2}$ are the ones contributing for $(\tau_{32})^{-1}$. The calculated radiative rates $(\tau_{31})^{-1}$ $(\tau_{32})^{-1}$ and the total (τ_3) lifetime of $^4G_{7/2}$ level for YLF and GLF crystals are shown in Table 1.

High-power and high-brightness diode lasers are efficient sources to promote nonlinear effects in laser media, for example up-conversion fluorescence. Using this effect, there is a variety of systems where the infrared pump radiation can be converted into visible fluorescence [20,22]. Most of the processes rely either on excited-state absorption of pumping radiation (ESAPR) or energy transfer up-conversion (ETU).

We have studied the pumping-related up-conversion processes in Nd YLF and GLF. The peak of the excited state absorption cross-section for the pumping radiation at 797 nm was evaluated as 2.4×10^{-22} cm^2 (GLF). A model to estimate the probability of the ETU process based on Förster–Dexter method was proposed and the ETU parameters were calculated. By solving the rate equations according to Ref. [23], for the system under continuous pumping, it was possible to estimate the up-conversion efficiency for different threshold populations for the two Nd systems. The ESAPR process does not have important effect on the up-conversion losses in Nd laser system, because this process involves a very small excited state absorption cross-section. Only the ETU processes ($K_{ETU} \cong 2.6 \times 10^{-14}$ N$_2$ for both crystals, YLF and GLF)
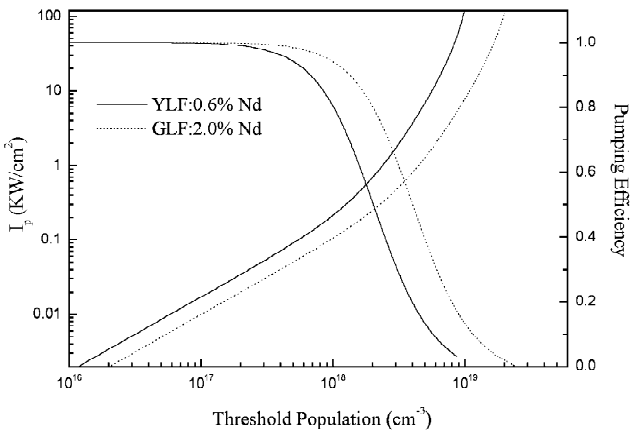

Fig. 2. Threshold pumping intensity (left-hand scale) and pumping efficiency (right-hand scale) as a function of the laser threshold population, for the laser crystals considered in the study.

are responsible for the nonlinear losses present in the system, for the threshold population above 5×10^{17} cm^{-3}. These processes cause important losses in the Nd laser system, increasing the power intensity to reach the laser threshold conditions.

The theoretical values for the threshold pumping intensity, as a function of the laser threshold population, are plotted in Fig. 2 (left scale) for the Nd:YLF and Nd:GLF crystals considered in this study. It can be seen that, due to the nonlinear up-conversion population losses, a threshold population above approximately 8.5×10^{18} cm^{-3} for YLF, and 2.1×10^{19} cm^{-3} for GLF cannot be obtained by raising the pumping intensity, for both systems. In this same figure, the normalized pumping efficiency as defined by [24] is plotted as a function of the threshold population (right scale). It is important to mention that the pumping intensity range covered by Fig. 3, corresponds to real possibilities of Nd-pumping intensities because it is always

Table 1
Relevant spectroscopic parameters for upper laser level population calculation, accounting for the up-conversion transition, in Nd:YLF and Nd:GLF

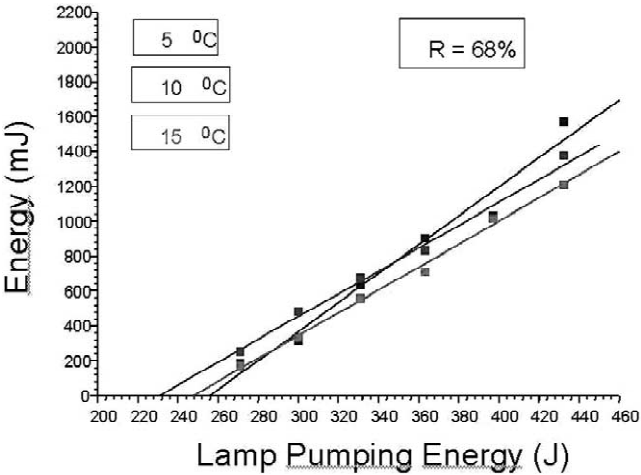|	YLF	GLF
[Nd] (cm^{-3})	8.5×10^{19}	2.85×10^{20}
σ_a (cm^2)	3.2×10^{-20}	2.1×10^{-20}
σ^* (cm^2)	6.4×10^{-22}	2.4×10^{-22}
	1.4×10^{-23}	
τ_2 (μs)	538	421
τ_3 (μs) ($^4G_{7/2}$)	150	183
τ_{31} (s^{-1})	3256	2974
τ_{32} (s^{-1})	186	196
Nd–Nd interaction	C_{D-A} (cm^6/s)	R_c (Å)
($^4F_{3/2}$/$^4F_{11/2}$)–1.05 μm	1.36×10^{-37}	20.4
($^4F_{3/2}$/$^4F_{13/2}$)–1.3 μm	1.83×10^{-37}	21.4

Fig. 3. Laser output energy as a function of the pumping energy for some relevant temperatures.

below the crystal breakdown intensity which is found to be of the order of 20 kW/cm^2 for Nd:YLF [25].

It is seen in Fig. 2 that the up-conversion processes impose dramatic limitations to the maximum achievable inverted population for the two systems. In both cases, the maximum inverted population is of the order of one-tenth of the total population. Therefore, higher Nd concentrations allow for higher gain coefficients, which favours the GLF crystal as a laser host, where a concentration of 5 mol% can be achieved. In these cases, the maximum gain is 2.6 cm^{-1} (1 mol%) for Nd:YLF and 6.7 cm^{-1} (5 mol%) for Nd:GLF, corresponding to the maximum population inversion of one-tenth of the total population available in both systems. It must be stressed that the pumping efficiencies for these systems, in this limit, are almost zero (see Fig. 2). In order to have 100% pumping efficiency and maximum gain, the maximum inverted populations are only 5×10^{17} and 1×10^{17} cm^{-3} for Nd:GLF and Nd:YLF, corresponding, respectively, to small gain coefficients of 0.05 and 0.02 cm^{-1}. In both cases these small gain coefficients are too small for practical systems where internal laser losses are inevitable and significant output mirror transmissions are often desirable. Long media (several cm long) can compensate these small gain coefficients, but in this case the great advantage of diode pumped systems, its compactness is lost. For the majority of the Nd laser systems, a trade off between pumping efficiencies and overall laser efficiency must be achieved.

The threshold pumping efficiency has great importance, for instance, in regenerative amplifiers and Q-switched lasers, that have a low Q period as part of their operation cycle. In both cases, the system must achieve the highest possible gain (inverted population), while compactness is also desired. This is specially important for Q-switched systems, where the pulse duration is a minimum for minimum cavity length and maximum initial gain ($2N_t\sigma_s l$). But, in order to achieve high optical efficiencies, one must minimize the nonlinear losses, so the gain coefficient must be kept moderate. Therefore, the present analysis can be very helpful when designing an optimized Q-switched Nd laser, allowing the determination of the best trade-off between pumping intensity and active medium length for maximum peak power and/or pulse energy. Once determined this optimum pumping intensity, the system is still scalable in energy by increasing the transverse active area. In the case of regenerative amplifiers even side pumping can be an advantageous alternative, because besides keeping the gain moderate (and therefore the optical efficiency high), presents less thermal problems. Finally, we must highlight the Nd:GLF as a promising laser medium for amplifier or Q-switched systems.

3.1.2. Ho systems

The Ho:LiYF$_4$ (Ho:YLF) laser at 2065 nm was obtained as a result of concentration optimization of the sensitizers

Er and Tm, based on a model comprising the various energy transfer mechanisms that take place in these long-lived metastable states. The laser output energy can be seen as a function of the pumping energy in Fig. 3.

The optimization process is based on a statistical description of the microscopic interaction among ions [26]. The microscopic parameters of energy transfer process can be described by a Förster–Dexter approach for resonant energy transfer and a modified model [27] for non-resonant energy transfer processes.

The description of the system allows one to estimate the transfer efficiency of a desired path of energy. There are three main paths of the pumping excitation energy to follow as can be seen in Fig. 4.

Both Er and Tm ions can transfer energy to the Ho ions. One can define the energy transfer efficiency as the ratio of the energy transfer probability normalized by the total deexcitation of the level and then plot the various efficiencies as a function of the ion concentrations. In Fig. 4 several paths of the energy transfer among ions can be seen.

In Fig. 5 the saturated transfer efficiency occurs for 10% of Tm. The optimized Tm concentration must be above or equal to 0.07 mol%. The Er–Ho energy transfer is maximized for Er concentrations greater than 0.1 (mol%) while the maximum Er–Tm energy transfer is reached for 0.15 (mol%). The Tm–Ho energy path is maximized for Tm concentration greater than 7%.

The maximization of the energy transfer from sensitizers to Ho must enclose all energy paths and the best concentrations were Er(40%):Tm(7%):Ho(0.4%) for small-signal gain greater than one.

These optimizations could indicate the best concentration for the Tm and Ho energy transfer and this choice
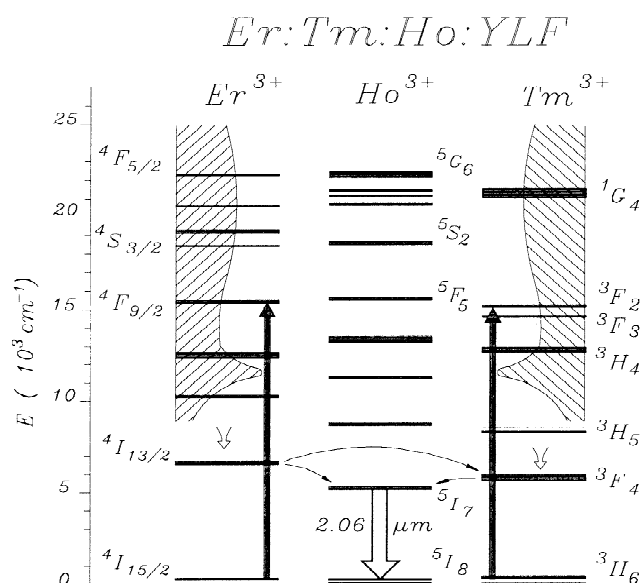

Fig. 4. Main pathways of energy transfer described in the energy level diagram.
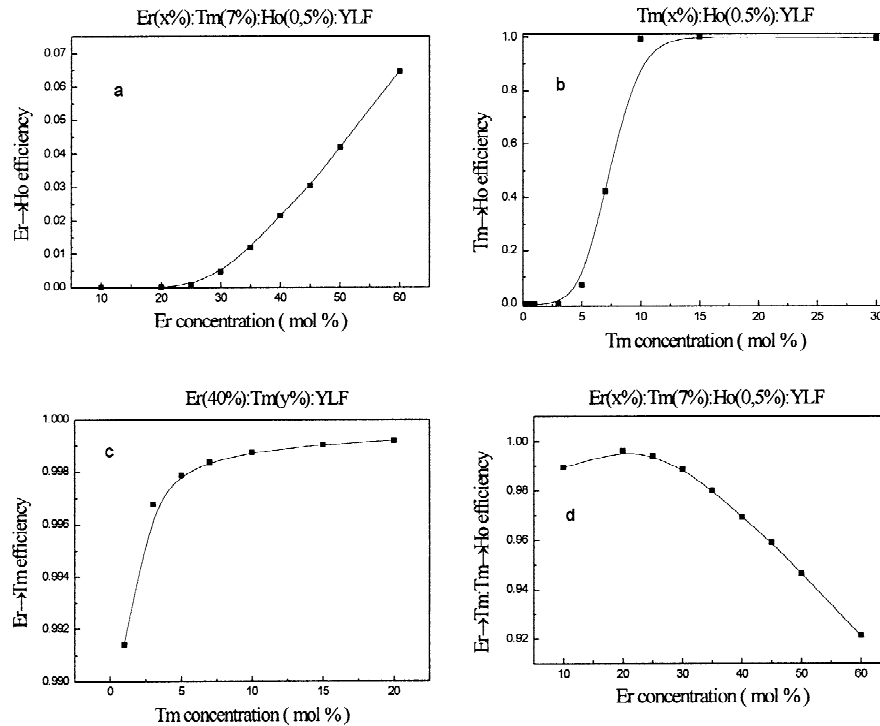
Fig. 5. Main energy transfer efficiencies for several energy pathways.

of concentrations resulted in a CW Ho laser with 2 W output, in a diode pumped system operation.

3.2. Laser performance

3.2.1. CW operation of the Nd:LuYLF and Nd:YLF lasers

The laser was pumped using a 20-W diode bar emitting at 792 nm which consists of 24 individual emitters in a linear array. It contains an anti-reflection coated collimating (cylindrical) fiber lens in the fast axis, which is factory installed in front of the array. The beam, with total emitting dimensions of $w_x = 1$ cm parallel to the bar and $w_y \approx 0.2$ mm perpendicular to the bar is highly elongated, nearly diffraction limited in the y-direction but more than 2000 times diffraction limited in the x-direction. It is therefore very difficult to focus this beam.

The two mirror beam-shaping technique [28,29] allows effective control of the beam-quality factors in the orthogonal x- and y-planes and, if desired, their equalization (Fig. 6). Basically, the beam shaper decomposes the highly elongated beam of the diode bar into 24 beams emitted by the individual emitters. These beams can be rearranged and stacked on top of each other [28]. In our case the beam was reconfigured into three columns of eight beams each as shown in the inset of Fig. 6. The reconfigured beam had dimensions and quality factors of $w_x = 200$ μm, $M_x^2 = 130$ and $w_y = 190$ μm, $M_y^2 = 85$ at the focus where the crystal is placed. With the diode bar emitting 20 W of output power, the pump power incident on the crystal was 14 W due to
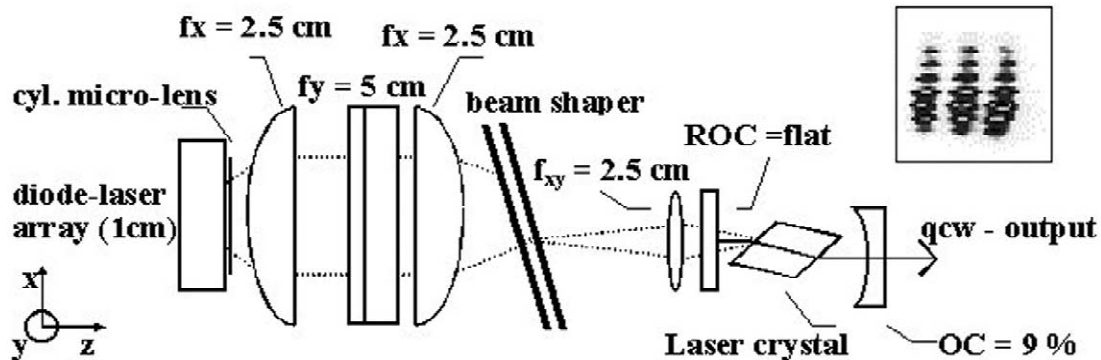

Fig. 6. Setup of the laser utilizing a two mirror beam shaper in the pump arrangement. The inset shows a photo of the pump distribution at the focus, taken with a CCD.
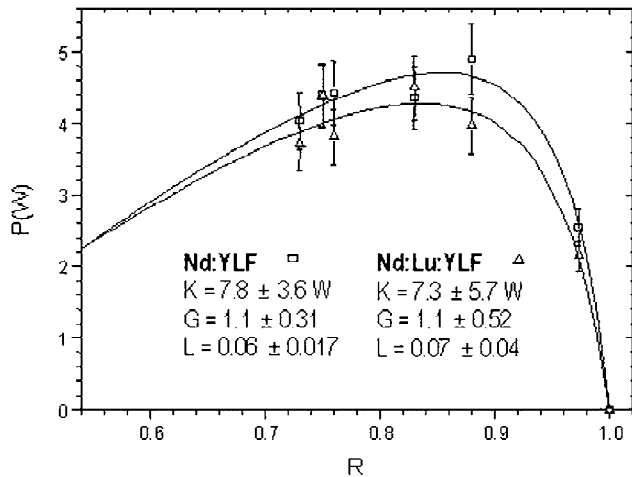
Fig. 7. Laser output power as a function of the mirror reflectivity.

losses in the beam shaper, lenses and the resonator input coupling mirror.

For the CW experiments, a 1-cm long, 0.009 (mol%) $Nd:Lu_{0.5}Y_{0.491}LF$ and a 0.013 (mol%) $Nd:Y_{0.987}LF$ sample of equal length were used (Fig. 7). The transmission of the laser samples around 1050 nm was better than 0.995(5) for both Nd:YLF and Nd:LuYLF laser crystals. The laser resonator consisted of a 1-m radius concave mirror, high reflector for 1050 nm, with 94% transmission for the pump beam, and flat output couplers with varied transmission at the laser wavelength. The total cavity length was 5 cm. Throughout most of the experiment, the duty cycle was only 10% due to a non-optimized crystal heatsink. Similar values for the maximum output power (4.5 ± 0.5 W), non-saturated gain (1.1 ± 0.5), and the round-trip cavity losses (0.06 ± 0.03) were achieved for both crystals as reported in Ref. [30], as seen in Fig. 7.

3.2.2. Mode-locked operation

Again, a two-mirror beam-shaper was used to produce a symmetrical beam. After the beam shaper, the pump beam was focused by a 50-mm spherical lens, producing an approximately circular beamwaist of 70 μm radius with quality factors $M_{x,y}^2 \approx 30$ and 3.8 W of pump power at the Nd:LuYLF crystal face.

The resonator was composed of two plane end mirrors, M_1 and M_2, and a set of two concave mirrors, M_3 and M_4, with 10-cm radius, to produce an additional intracavity focus in the central arm of the resonator, as shown in Fig. 8. At the middle of this central arm a 1-cm long sample of SF57 glass was inserted at Brewster angle. The Nd:LuYLF crystal was positioned 8 mm from mirror M_1, that has a high transmission for $\lambda_P = 792$ nm and is a high reflector (HR) for the laser emission. A home-made, Brewster-angled acousto-optical modulator was inserted in the cavity, close to mirror M_2, to provide an auxiliary amplitude modulation to initiate and sustain the mode-locking regime even in the presence of instabilities. The central arm length was adjusted to $L_M \cong 11.4$ cm, favoring the Kerr-lens sensitivity of the resonator [31], and providing a suitable beamwaist at mirror M_1, which leads to the best matching with the pumped volume. To compensate for the group velocity dispersion, a Gires-Tournois interferometer (GTI) was used as the second end mirror (M_2). This element consists of two plane mirrors, one with reflectivity $R \approx 100\%$ and the other with $R = 4\%$. The distance between the mirrors can be adjusted in order to make the roundtrip inside the GTI much shorter than the expected pulse length. This distance was kept around $d \approx 350$ μm, which corresponds to a dispersion of -2 ps^2 at anti-resonance. The low reflectivity mirror position is piezoelectrically driven, allowing adjustments in the phase. Fine-tuning of the KLM laser operation was accomplished while observing pulse stabilization and shortening by using an electronic detection system with total response time of 24 ps.

In a previous work [32], we reported the stable generation of 6-ps pulses from an all-solid-state KLM Nd:YLF laser with weak acousto-optical modulation. In that case, the time-bandwidth product was $\Delta\nu\tau_P \cong 0.54$. The pulsewidth obtained from the KLM Nd:LuYLF laser was shorter as expected due to its larger bandwidth. In this case, the auto-correlation measurement has revealed a full-width at half maximum (FWHM) of 4.5 ps and a time-bandwidth product of $\Delta\nu\tau_P \cong 0.5$ was measured [33].

3.2.3. Laser operation of the Tm:Ho:YLF laser

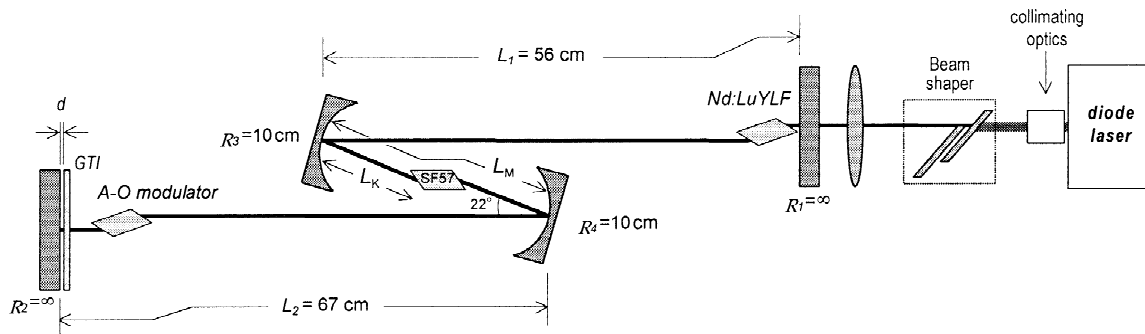Pumping was achieved by the 20 W diode laser, as described in Section 3.2.1.

Fig. 8. System setup for the all solid-state KLM Nd:LuYLF laser.

The laser resonator consisted of a flat, high reflecting mirror for 2.06 μm, which had 90% transmission for the pump beam and a curved output coupler with an optimized 9% transmission at the laser wavelength. The cavity length was held at 3 cm but remains stable up to a length of 9.5 cm (however, with additional 10% loss attributed to water absorption). The output coupler's radius of curvature (ROC) of 10 cm produces a beam waist of 170 μm inside the Brewster cut crystal for the 2.06-μm fundamental transversal mode (TEM$_{00}$).

Experimentally it was confirmed that a lower than 0.01 (mol%) Ho concentration and 5.5-mm length laser crystal presented the best compromise between efficient pump absorption and small reabsorption losses. The pumping was tuned to the Tm absorption at 792 nm.

Keeping the crystal heatsink at room temperature, while varying the duty cycle of the diode bar, we achieved a best result of 2 W of peak output power at 10% duty cycle. At higher duty cycles we verified a loss in laser efficiency. The operation at higher duty cycles raises the local crystal temperatures and the observed drop in laser efficiency points out that the main loss mechanism of this laser crystal is due to the increase in ground state population and thus reabsorption. At this condition, the increase in ground state population leads to an almost equivalent performance as the higher Ho concentration crystals under low-duty cycle pumping. We also observed the same effect (and it was particularly strong) when using the crystals with higher Ho concentration (1%). Lowering the crystal temperature and keeping the diode emission wavelength at 792 nm, the laser can sustain its efficiency at duty cycles higher than 10%. When the crystals temperature is lowered from 10 to −27 °C, the duty cycle may be increased to a maximum of 60% without substantial power loss as can be seen in Fig. 9.

4. Summary

We have studied the growth of Nd doped mixed crystals of LiY$_x$Lu$_{1-x}$F$_4$ and the emission bandwidth in order to optimize the Lu concentration and still maintain a broad emission band. The ideal concentration is 50% and the corresponding emission bandwidth is 25% larger than in the LiYF$_4$ system. The crystals have shown good optical quality and CW laser action was obtained, with an output power of 4.5 W for pumping with 14 W of a diode laser. The gain obtained with this crystal was comparable to the Nd:YLF system. We have also obtained mode-locked operation in the KLM regime and typical pulse width is 4.5 ps, much smaller than the same laser scheme for Nd:YLF (6 ps). In both cases, we could not take advantage of the total emission bandwidth that could lead to pulses shorter than 1 ps.

Concerning the Ho:Tm:YLF laser medium, we could establish a theoretical model that takes into account the energy transfer mechanism between Ho and Er and Tm, and based on it, we have determined the optimal concentrations of the Ho and Tm ions of 0.4 and 6 mol%, respectively. Good optical quality crystals were obtained and, in the CW laser operation, 2 W of average power were taken out of the 9 W, diode pumped system. We could run the laser in two ways: with a duty cycle of 10%, without cooling and with 60% duty cycle, cooled, which is remarkable for a quasi-three-level system.
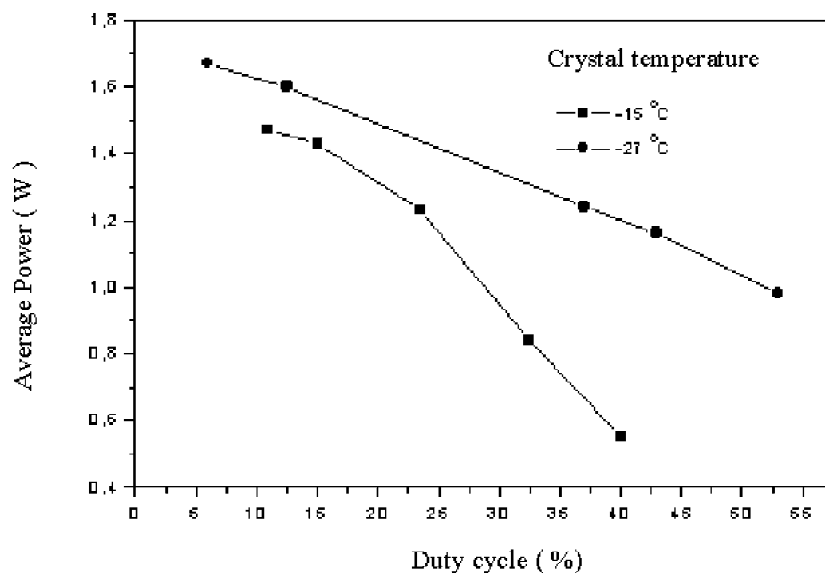
Fig. 9. Average power for two different temperatures on a duty cycle.

References

[1] B.H. Stevens, H.O. Trowbridge, G. Harrison, S.F. Silverton, J. Endodont. 20 (1994) 246.

[2] J.M. White, H.E. Goodis, G.W. Marshall Jr., S.J. Marshall, Scan. Microsc. 7 (1993) 239.

[3] A. Finch, J. Flint, CLEO'95, Tech. Digest Series 15, Paper CWH2 (1995) 232.

[4] J. Yu, U.N. Singh, N.P. Barnes, M. Petros, Opt. Lett. 10 (1998) 781.

[5] N.P. Barnes, K.E. Murray, M.G. Jani, Appl. Opt. 36 (1997) 3363.

[6] G. Rustad, K. Stenersen, IEEE J. Quant. Electron. 32 (1996) 1645.

[7] J.J. Degnan, IEEE J. Quant. Electron. 25 (1989) 214.

[8] I.M. Ranieri, K. Shimamura, K. Nakano, T. Fujita, L.C. Courrol, S.P. Morato, T. Fukuda, J. Crystal Growth 217 (2000) 145.

[9] I.M. Ranieri, K. Shimamura, K. Nakano, T. Fujita, T. Fukuda, Z. Liu, N. Sarukura, J. Crystal Growth 217 (2000) 151.

[10] S.L. Baldochi, K. Shimamura, K. Nakano, Na. Mujilatu, T. Fukuda, J. Crystal Growth 205 (1999) 537.

[11] I.M. Ranieri, S.L. Baldocchi, A.M.E. Santo, L. Gomes, L.C. Courrol, L.G. Tarelho, W. de Rossi, J.R. Berretta, F.E. Costa, G.E.C. Nogueira, N.U. Wetter, D.M. Zezell, N.D. Vieira Jr., S.P. Morato, J. Crystal Growth 166 (1996) 423.

[12] E.P. Maldonado, N.D. Vieira Jr., J. Opt. Soc. Am. B 12 (1995) 2482.

[13] L.A. Riseberg, W.C. Holton, J. Appl. Phys. 43 (1972) 1876.

[14] N.P. Barnes, B.M. Walsh, K.E. Murray, G.J. Quarles, V.K. Castillo, TOPS 10 (1997) 448.

[15] E.P. Ippen, Appl. Phys. B 58 (1994) 159.

[16] H.A. Haus, J.G. Fujimoto, E.P. Ippen, J. Opt. Soc. Am. B 8 (1991) 2068.

[17] D.E. McCumber, Phys. Rev. 136 (1964) 954.

[18] X.X. Zhang, M. Bass, A.B. Villaverde, J. Lefaucher, A. Pham, B.H.T. Chai, Appl. Phys. Lett. 62 (1993) 1197.

[19] E.P. Maldonado, I.M. Ranieri, S.P. Morato, N.D. Vieira Jr., ASSL 10 (1997) 444.

[20] C.Y. Chen, W.A. Sibley, D.C. Yeh, C.A. Hunt, J. Luminesc. 43 (1989) 185.

[21] C. Li, Y. Guyot, C. Linares, R. Moncorgé, M.F. Joubert, OSA Proc. Adv. Solid-State Lasers 15 (1993) 9195.

[22] R.M. Macfarlane, F. Tong, A.J. Silversmith, W. Lenth, Appl. Phys. Lett. 52 (1988) 1300.

[23] L.C. Courrol, E.P. Maldonado, L. Gomes, N.D. Vieira Jr., I.M. Ranieri, S.P. Morato, Opt. Mat. 14 (2000) 81.

[24] Y. Guyot, H. Manaa, J.Y. Rivoire, R. Moncorgé, N. Garnier, E. Descroix, M. Bom, P. Laporte, Phys. Rev. B 51 (1995) 784.

[25] M. Lopes Filho, Master Dissertation, IPEN/CNEN-SP, 1999.

[26] Instituto de Pesquisas Energéticas e Nucleares; D.M. Zezzel, I.M. Ranieri, L. Gomes, L.C. Courrol, L.V.G. Tarelho, M.B. Camargo, N.D. Vieira Jr., S.P. Morato, W. Rossi, Optimization of active holmium laser material containing erbium and thulium ions by zone refining in hydrofluoric acid, 1998. Br Pat. N. BR9600093-A.

[27] L.V.G. Tarelho, L. Gomes, I.M. Ranieri, Phys. Rev. B 56 (1997) 14344.

[28] N.U. Wetter, Opt. Laser Technol. 33 (2001) 181.

[29] W.A. Clarkson, D.C. Hanna, Opt. Lett. 21 (1996) 375.

[30] E.P. Maldonado, N.U. Wetter, I.M. Ranieri, E.A. Barbosa, L.C. Courrol, S.P. Morato, N.D. Vieira Jr., Crystal growth, OSA Trends Opt. Photonics 26 (1999) 642.

[31] V. Magni, G. Cerullo, S. De Silvestri, A. Monguzzi, J. Opt. Soc. Am. B 12 (1995) 476.

[32] E.P. Maldonado, N.D. Vieira Jr., Rev. Fís. Appl. Instrum. 12 (1998) 102.

[33] E.P. Maldonado, E.A. Barbosa, N.U. Wetter, L.C. Courrol, I.M. Ranieri, S.P. Morato, N.D. Vieira Jr., Opt. Eng. 40 (2001) 1573.